

INFLUENCE OF ZIGZAG TAPE–INDUCED TRANSITION ON THE DU89-134 AIRFOIL PERFORMANCE AT LOW REYNOLDS NUMBER

Matija Avirović[1,2,3], Carlo Brunelli[1,3,4], Benoît G. Marinus[1], Joris Degroote[2,5], Jeroen van Beeck[3] & Emile Van Vaerenbergh[1]

[1]Royal Military Academy, Brussels, Belgium
[2]Ghent University, Ghent, Belgium
[3]Von Karman Institute for Fluid Dynamics, Sint-Genesius-Rode, Belgium
[4]Vrije Universiteit Brussel, Brussels, Belgium
[5]Flanders Make, Ghent, Belgium

Abstract

Force, pressure, and surface temperature measurements were used to investigate the influence of zigzag tape on the aerodynamic performance of the DU89-134 airfoil at chord-based Reynolds numbers of $\mathrm{Re}_c = 2.5 \times 10^5$ and $\mathrm{Re}_c = 5 \times 10^5$, corresponding to critical Reynolds numbers Re_k of approximately 180 and 420, respectively. A significant improvement in aerodynamic performance was observed for the tripped airfoil at the lower Reynolds number. This improvement was attributed to the near-optimal critical Reynolds number, which enabled the zigzag tape to effectively promote transition and thereby substantially reduce the extent of the separated region. In contrast, no performance improvement was observed at the higher Reynolds number. This was attributed to the limited influence of the laminar separation bubble on the baseline flow, which reduced the potential for improvement through forced transition, and to the higher critical Reynolds number ($\mathrm{Re}_k \approx 420$), which, in turn, diminished the effectiveness of the zigzag tape and resulted in a slight drag penalty at higher angles of attack.

Keywords: Airfoil, Zigzag tape, Laminar separation bubble, Infrared termography

1. Introduction

Airfoils operating in the low Reynolds number flow regime often experience suction-side laminar boundary layer separation and the formation of a separated shear layer due to adverse pressure gradients and weak near-wall streamwise momentum. The resulting separated shear layer is inherently unstable and, depending on the flow conditions, may either remain separated or undergo a rapid transition from laminar to turbulent flow through disturbance amplification, eventually reattaching to the airfoil surface to form a Laminar Separation Bubble (LSB) [1, 2, 3, 4]. Flow separation and the presence of an LSB are often linked to the degradation of airfoil performance in the low-Reynolds-number regime, primarily due to increased pressure drag and, to a lesser extent, reduced lift [5, 6, 7, 8].

To mitigate the adverse effects of flow separation and LSBs, boundary layer tripping devices are commonly used [8, 9, 10]. Methods such as distributed roughness elements, vortex generators, trip wires, and zigzag tape introduce sufficiently strong disturbances into the laminar boundary layer, promoting earlier transition to turbulence. The resulting turbulent boundary layer exhibits enhanced momentum exchange near the wall and is therefore less susceptible to adverse pressure gradients, reducing the likelihood of separation and LSB formation. For a tripping device to be effective, the associated reduction in airfoil pressure drag must outweigh the additional pressure drag introduced by the device itself and the increased skin-friction drag of the turbulent boundary layer. Furthermore,

the effectiveness of boundary layer tripping is strongly dependent on the trip geometry and chordwise location, and no universally optimal configuration exists [10, 11].

Zigzag tape has attracted interest as a boundary layer tripping device due to its ability to induce transition at relatively low critical Reynolds numbers ($\mathrm{Re}_k \approx 200$) [9, 12, 13, 14], allowing effective boundary layer tripping while maintaining a small geometric height and limiting the associated drag penalty. The transition mechanism associated with zigzag tape involves the formation of a separated flow region immediately downstream of the tape, accompanied by an unstable shear layer and the generation of streamwise-oriented vortical structures [15, 16, 17, 14]. These flow structures promote rapid breakdown of the laminar boundary layer, leading to early transition to turbulence and subsequent reattachment of the now turbulent shear layer to the surface.

The aerodynamic effects of zigzag tape on low-Reynolds-number airfoils have been investigated in a limited number of studies. Multiple zigzag tape configurations were experimentally investigated on the Eppler 374 airfoil at $\mathrm{Re}_c = 2 \times 10^5$, with drag reductions reported for most configurations relative to the clean airfoil [11]. The study further showed that airfoils exhibiting large LSBs benefit most from boundary layer tripping due to the associated reduction in pressure drag. Experimental investigations on the SD7032 airfoil at $\mathrm{Re}_c = 1 \times 10^5$ and 2×10^5 demonstrated that zigzag tape can effectively suppress or reduce LSBs and improve airfoil performance [12]. Complementary experimental and numerical investigations on SD7032 airfoil further showed that the aerodynamic effectiveness of zigzag tape depends on the critical Reynolds number, with optimum performance typically obtained in the range $150 < \mathrm{Re}_k < 250$ [14].

The present study therefore investigates the influence of zigzag tape–induced transition on the aerodynamic performance of the DU89-134 airfoil [18]. Previous investigations of the DU89-134 airfoil demonstrated a significant deterioration in aerodynamic performance at low Reynolds numbers compared to the original design Reynolds number, primarily associated with suction-side flow separation and the formation of large LSBs [19, 20]. In particular, the reduction in Reynolds number was shown to increase the extent of separated flow and associated pressure drag, motivating the present investigation into whether zigzag tape can suppress or reduce laminar separation and improve aerodynamic performance under low-Reynolds-number operating conditions. The DU89-134 airfoil was selected due to its close geometrical similarity to an airfoil used in a High-Altitude Pseudo-Satellite (HAPS) flight demonstrator currently under development, making the present investigation directly relevant to the intended application.

2. Experimental setup and methodology

2.1 Wind tunnel and airfoil model

Force, pressure, and surface temperature measurements were conducted in the low-speed, low-turbulence, open-circuit wind tunnel of the Royal Military Academy. The wind tunnel features a contraction ratio of 9:1 and a closed test section (Fig. 1) with a length of $1.2\,\mathrm{m}$ and a cross-sectional area of $0.6\,\mathrm{m} \times 0.6\,\mathrm{m}$. The free-stream velocity in the test section can be continuously regulated between 0 and $45\,\mathrm{m\,s^{-1}}$, while the turbulence intensity within the test section remains below 0.2 % over the operational range of the facility [21].

The experiments were conducted at chord-based Reynolds numbers of $\mathrm{Re}_c = 2.5 \times 10^5$ and 5.0×10^5 for angles of attack ranging from $-3^\circ \leq \alpha \leq 6^\circ$. The airfoil angle of attack was adjusted using the rotary table located underneath the test section, while the reference zero-angle position was established using a dedicated 3D-printed alignment jig. The complete wind tunnel test matrix is provided in Table 1.

The DU89-134 airfoil model, with a chord length of $c = 0.2\,\mathrm{m}$ and a span of $s = 0.595\,\mathrm{m}$, was assembled from three segments. Each segment was fabricated from Grey Resin V4 using a Formlabs Form 3 stereolithography 3D printer with a layer height of $0.05\,\mathrm{mm}$. To minimize the influence of surface roughness on boundary-layer transition, the airfoil surface was polished to an average surface roughness of $R_a = 0.2\,\mu\mathrm{m}$. Zigzag tape with a thickness of $0.3\,\mathrm{mm}$ was applied over the full airfoil span, with the trailing edge of the tape positioned at either $x/c = 0.4$ or $x/c = 0.5$, as shown in Fig. 2a. The critical Reynolds number, Re_k, based on the flow velocity at the zigzag tape height [22], was estimated from the velocity profiles measured over the DU89-134 airfoil in [19], corresponding to approximately 180

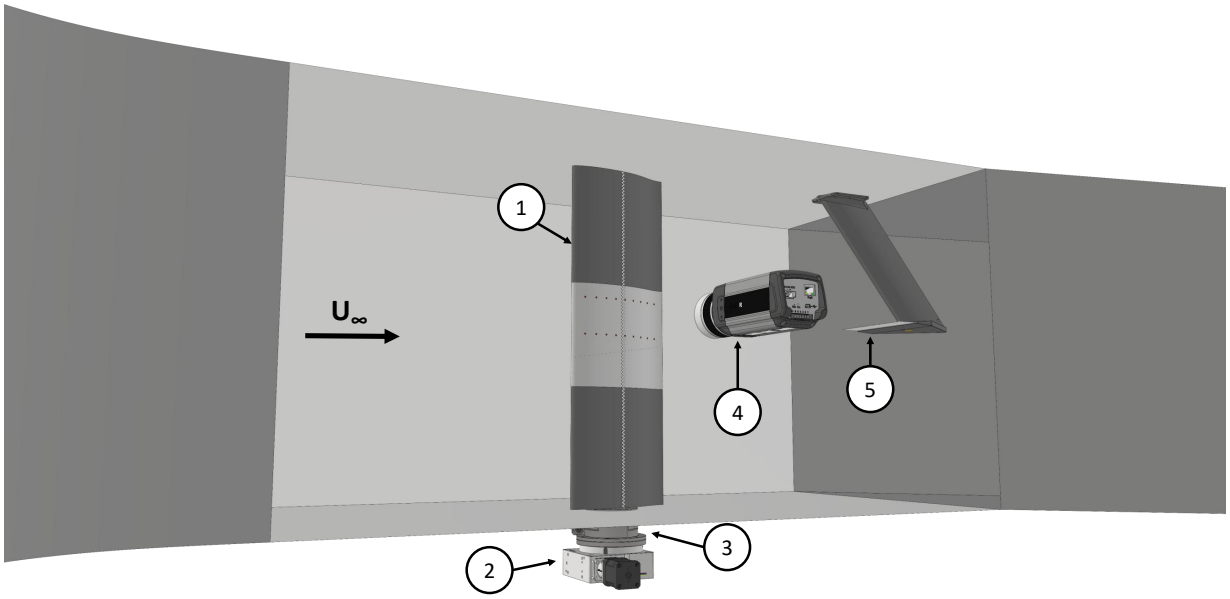


Figure 1 – Wind tunnel test section showing: (1) DU89-134 airfoil, (2) rotary table, (3) force-torque transducer, (4) infrared camera, and (5) wake rake.

for $\mathrm{Re}_c = 2.5 \times 10^5$ and 420 for $\mathrm{Re}_c = 5 \times 10^5$.
The middle airfoil section was designed to accommodate an internally mounted heating element that provided the required heat flux for the infrared thermography measurements. In addition, 18 copper fiducial markers were applied to the suction side of the airfoil to facilitate infrared image perspective correction. The same section also incorporated 49 integrated pressure taps, each with a surface diameter of $0.7\,\mathrm{mm}$. To minimize the influence of upstream pressure taps on downstream measurements, the pressure tap orifices were inclined at an angle of 8° relative to the airfoil chord. The locations of the heating element and fiducial markers, together with the pressure tap geometry, are shown in Fig. 2a. The pressure tap distribution over the suction and pressure sides of the airfoil is presented in Fig. 2b, where pressure taps that became obstructed during manufacturing are indicated by crosses.

Table 1 – Wind tunnel test matrix

Airfoil configuration	**M**	$\mathbf{Re_c}$	$\mathbf{Re_k}$	α [°]
Clean airfoil Zigzag 0.4c Zigzag 0.5c	0.05 0.10	2.5×10^5 5.0×10^5	≈ 180 ≈ 420	-3 to 6

2.2 Force measurements

Aerodynamic forces were measured using an ATI Delta 6-axis force-torque transducer mounted on the rotary table underneath the wind tunnel test section, as shown in Fig. 1. The transducer provided force measurements in the airfoil-fixed coordinate system, from which lift (L) and drag (D) were obtained by transformation to the flow coordinate system using equations 1 and 2.

$$L = F_y \cos\alpha - F_x \sin\alpha \tag{1}$$

$$D = F_y \sin\alpha + F_x \cos\alpha \tag{2}$$

where, F_x and F_y denote the force components parallel and perpendicular to the airfoil chord, while α represents the angle of attack.

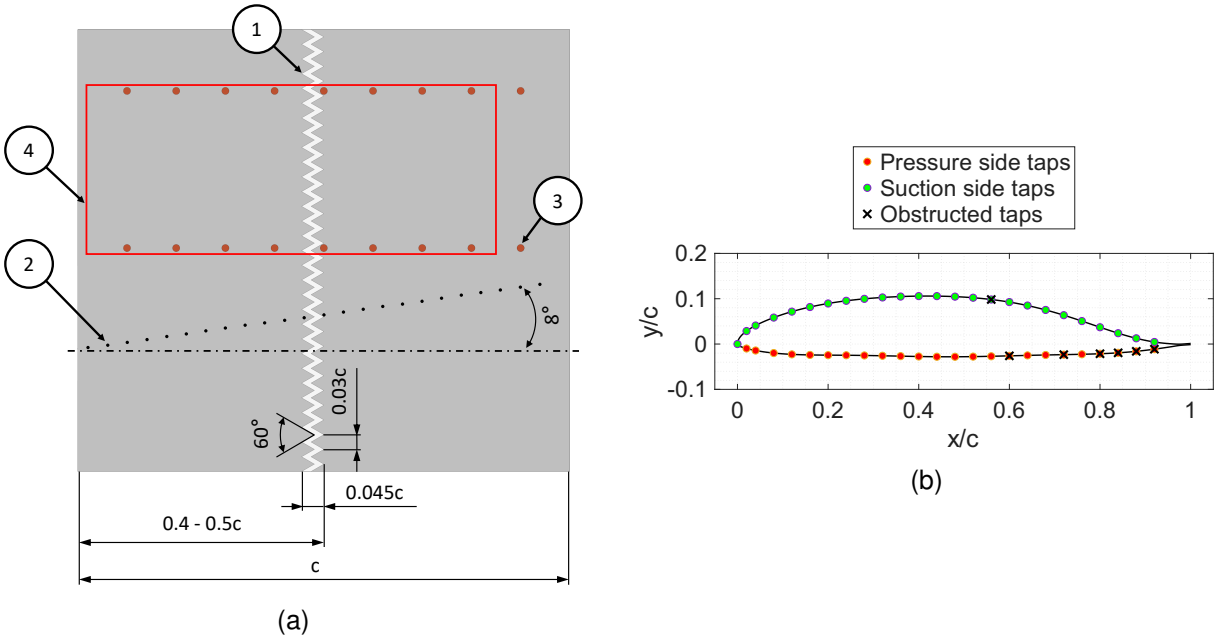


Figure 2 – (a) Detail of the airfoil suction side showing: (1) zigzag tape, (2) suction-side pressure taps, (3) fiducial markers, and (4) the position of the internal heating element. (b) Chordwise distribution of pressure taps on the airfoil surface. Green markers indicate suction-side taps, red markers indicate pressure-side taps, and crosses denote obstructed taps.

The measurement uncertainty of both force components was 1% of the transducer's full-scale range, while the uncertainty associated with the angle-of-attack setting of the rotary table was less than 0.1°. Propagation of these uncertainties resulted in lift- and drag-coefficient uncertainties of approximately ± 0.02 for $\mathrm{Re}_c = 2.5 \times 10^5$ and ± 0.005 for $\mathrm{Re}_c = 5 \times 10^5$, with a 95% confidence interval.
In addition to force-torque transducer measurements, the airfoil profile drag coefficient was determined using the momentum-deficit method described in [1]. Wake total-pressure measurements were acquired using the wake rake shown in Fig. 1, which comprised 48 total-pressure ports spaced $3.5\,\mathrm{mm}$ apart and positioned 2.5 chord lengths downstream of the airfoil trailing edge. The pressure ports were connected to two SVM Tech PSC24 differential pressure scanners with a measurement range of $\pm 2500\,\mathrm{Pa}$. Propagation of the measurement uncertainties resulted in drag-coefficient uncertainties of ± 0.004 for $\mathrm{Re}_c = 2.5 \times 10^5$ and ± 0.002 for $\mathrm{Re}_c = 5 \times 10^5$, with a 95% confidence interval.
Measured lift and drag coefficients, and the angle of attack were adjusted for solid blockage, wake blockage and streamline curvature correction, which were applied as described in [23].

2.3 Surface pressure measurements

Steady surface pressure measurements were acquired from the pressure taps using the same differential pressure scanners employed for the wake integration measurements. The airfoil pressure taps were connected to the pressure scanners using brass tubing near the airfoil surface and silicone tubing downstream, resulting in a total tubing length of approximately $1\,\mathrm{m}$. For each airfoil configuration and angle of attack, the pressure signals were recorded over a duration of $1\,\mathrm{min}$ at a sampling frequency of $10\,\mathrm{Hz}$. The recorded pressure data were subsequently time-averaged to determine the corresponding pressure coefficients. The pressure coefficient measurement uncertainty has been calculated to be smaller than ± 0.15 for $\mathrm{Re}_c = 2.5 \times 10^5$ and smaller than ± 0.04 for $\mathrm{Re}_c = 5 \times 10^5$ with a 95% confidence interval.

2.4 Surface temperature measurements

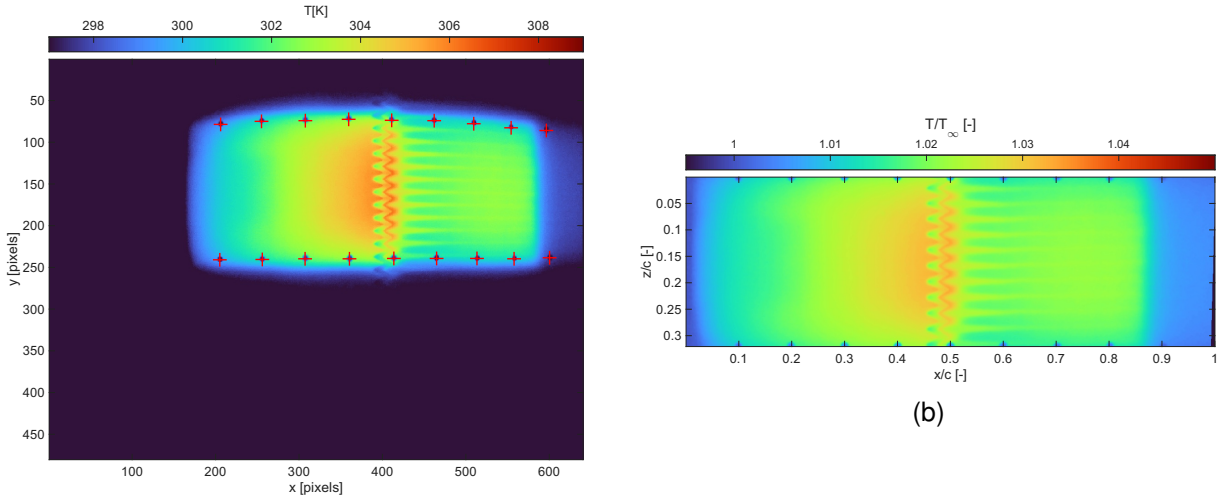
Airfoil suction-side surface temperature distributions were acquired using a FLIR A655sc long-wave infrared camera operating in the $7.5\,\mu\mathrm{m}$ to $14\,\mu\mathrm{m}$ spectral range and equipped with an uncooled microbolometer detector. The camera has a Noise Equivalent Temperature Difference (NETD) below $30\,\mathrm{mK}$ and a spatial resolution of 640×480 pixels. During the experiments, the camera was positioned

perpendicular to the airfoil chord at a distance of $0.3\,\mathrm{m}$, with its field of view centered on the airfoil mid-span, as shown in Fig. 1.

To establish a temperature difference between the airfoil surface and the freestream flow, the internal heating element was operated at a constant voltage of $24\,\mathrm{V}$ and a current of $0.1\,\mathrm{A}$, corresponding to an electrical power of $2.4\,\mathrm{W}$ and an average surface heat flux of approximately $300\,\mathrm{W\,m^{-2}}$.

For each flow condition, 150 infrared images were recorded at the camera's maximum acquisition frequency of $30\,\mathrm{Hz}$, corresponding to $5\,\mathrm{s}$ of flow time. To minimize image distortion resulting from changes in airfoil angle of attack, the raw infrared images (Fig. 3a) were geometrically corrected and projected onto a 640×2000 computational grid. The correction procedure was based on detecting the fiducial marker centers using the Hough transform [24] and aligning them with the corresponding reference marker locations known a priori from the airfoil CAD model (Fig. 3b).

The corrected infrared images were subsequently time- and span-averaged to obtain the mean chordwise temperature distribution and temperature gradient. These quantities were then used to identify the flow separation, transition, and reattachment locations according to the procedure described in [3].



(a) (b)

Figure 3 – Comparison between (a) the raw infrared image, where red crosses indicate the detected fiducial marker centers, and (b) normalized surface temperature distribution projected onto the airfoil coordinate system using the fiducial markers.

3. Results and discussion

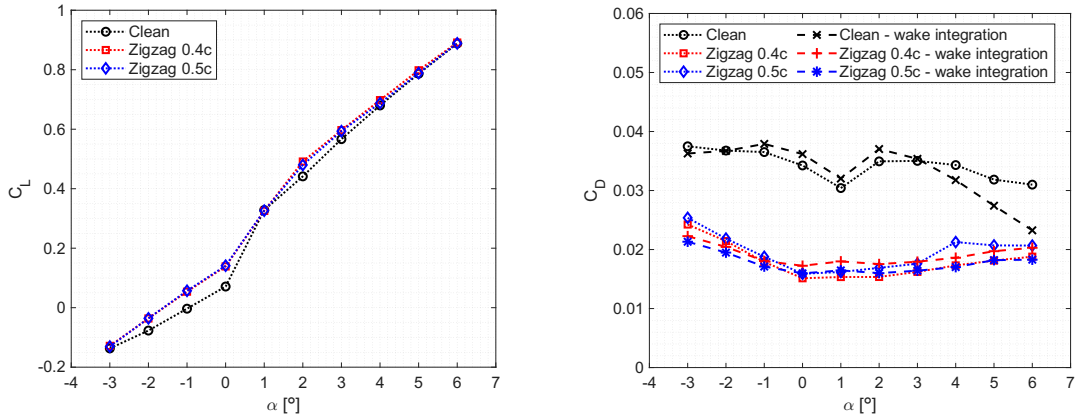
3.1 Airfoil performance

Lift and drag coefficients for the clean airfoil and the airfoil equipped with zigzag tape at $x/c = 0.4$ and $x/c = 0.5$ for $\mathrm{Re}_c = 2.5 \times 10^5$, obtained from force-balance measurements, are shown in Fig. 4. In addition, drag coefficients obtained from wake integration are included for comparison in Fig. 4b.

It can be observed that, at this Reynolds number, the zigzag tape has a minor influence on the lift coefficient but a pronounced effect on the drag coefficient. The maximum absolute difference in lift coefficient, between the clean and tripped configurations, is on the order of $\Delta C_L \approx 0.07$ at $\alpha = 0^\circ$.

For the drag coefficient, the force-balance measurements indicate differences between the clean airfoil and the tripped configurations on the order of $\Delta C_D \approx 0.015$ across the entire range of α, corresponding to approximately a factor-of-two reduction in drag. Differences between the two zigzag tape positions are small and fall within the measurement uncertainty, and are therefore not considered statistically significant.

The wake integration results support the findings of the force-balance measurements, showing good agreement in terms of overall trends and relative differences between configurations. In particular, the significant drag reduction associated with the zigzag tape is consistently captured. Minor discrepancies are observed, with the wake integration generally yielding slightly lower drag coefficients for

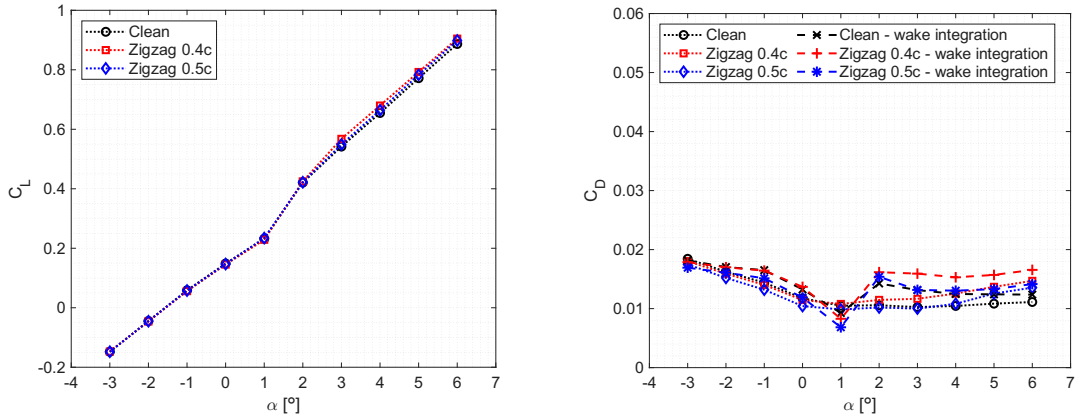


(a) (b)

Figure 4 – Lift (a) and drag (b) coefficients in relation to angle of attack for $\mathrm{Re}_c = 2.5 \times 10^5$.

the clean configuration at higher angles of attack; however, these differences do not affect the overall conclusions.

For $\mathrm{Re}_c = 5 \times 10^5$, the lift and drag coefficients are shown in Fig. 5. At this Reynolds number, the zigzag tape has a negligible effect on the lift coefficient and only a minor influence on the drag coefficient. The maximum absolute difference in lift coefficient between the clean and tripped configurations is $\Delta C_L \approx 0.02$, occurring at $\alpha = 3°$.



(a) (b)

Figure 5 – Lift (a) and drag (b) coefficients in relation to angle of attack for $\mathrm{Re}_c = 5 \times 10^5$.

Similarly, differences in drag are small across the entire range of α. The tripped configurations exhibit slightly higher drag than the clean airfoil at higher angles of attack, with a maximum difference of $\Delta C_D \approx 0.003$ at $\alpha = 6°$. While this difference is of the same order as the experimental uncertainty, its magnitude remains small. No conclusive performance difference between the two zigzag tape positions can therefore be identified.

As in the lower Reynolds number case, the wake integration results support the findings of the force-balance measurements, reproducing the overall trends. An exception is observed at $\alpha = 1°$, where a pronounced dip in the drag coefficient is obtained from wake integration. This behaviour is accompanied by the presence of a high-pitch tonal noise, which has previously been attributed to separation near the pressure-side trailing edge at $\mathrm{Re}_c = 1.5$–3×10^6 [18]. It is hypothesised that this behaviour enhances mixing in the wake and promotes the entrainment of higher-momentum flow into the wake deficit, leading to an underestimation of the drag coefficient when using the momentum-deficit method. Furthermore, the application of zigzag tape near $x/c = 0.9$ on the pressure side of the airfoil resulted in a significant reduction in tonal noise, providing additional evidence that the noise is associated with trailing-edge separation. The aerodynamic consequences of this modification,

however, were not quantified in the present study.
Figure 6 presents the drag polar comparison for the clean and tripped airfoil configurations at $\mathrm{Re}_c = 2.5 \times 10^5$ and $\mathrm{Re}_c = 5 \times 10^5$. Given the close agreement between wake integration and force-balance measurements, the drag coefficients obtained from wake integration are omitted for clarity.

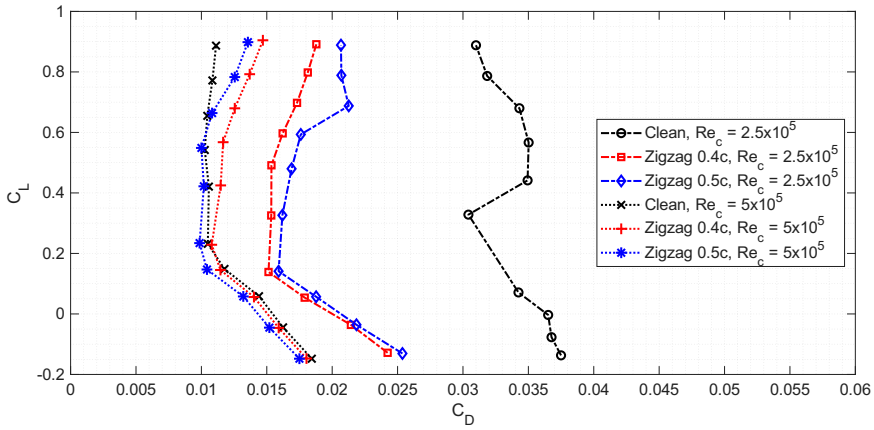
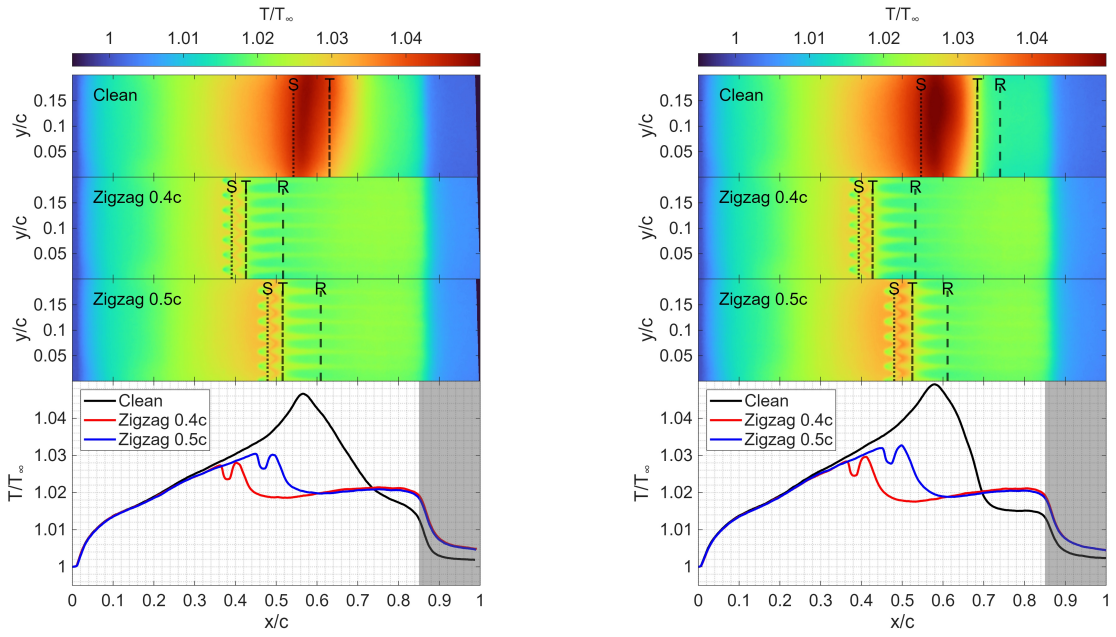


Figure 6 – Drag polar comparison for clean airfoil and airfoil with zigzag tape for $\mathrm{Re}_c = 2.5 \times 10^5$ and $\mathrm{Re}_c = 5 \times 10^5$.

At $\mathrm{Re}_c = 2.5 \times 10^5$, the application of zigzag tape results in a pronounced shift of the drag polar towards lower drag coefficients across the entire lift range, indicating a significant improvement in aerodynamic performance. The difference between the clean and tripped configurations is substantial, consistent with the drag reduction previously observed. Notably, the drag polar of the tripped configurations at $\mathrm{Re}_c = 2.5 \times 10^5$ approaches that of the clean airfoil at $\mathrm{Re}_c = 5 \times 10^5$, indicating that boundary-layer tripping effectively mitigates low-Reynolds-number performance penalties.
In contrast, at $\mathrm{Re}_c = 5 \times 10^5$, the drag polars for the clean and tripped configurations collapse closely together, indicating that the influence of zigzag tape on aerodynamic performance is minimal. A slight drag penalty is observed for the tripped configurations in the high-lift regime; however, the magnitude of the effect remains small and is generally comparable to the measurement uncertainty. No clear performance advantage associated with either zigzag tape position can therefore be identified.
This behaviour can be interpreted in terms of the critical Reynolds number associated with the zigzag tape. At $\mathrm{Re}_c = 2.5 \times 10^5$, the estimated value of $\mathrm{Re}_k \approx 180$ lies close to the optimal range reported in the literature ($\mathrm{Re}_k \approx 200$), for which maximum drag reduction is achieved [12, 14]. Conversely, at $\mathrm{Re}_c = 5 \times 10^5$, the higher value of $\mathrm{Re}_k \approx 420$ corresponds to a supercritical regime, where the additional device drag of the tape offsets any potential benefit of forced transition.

3.2 Flow topology

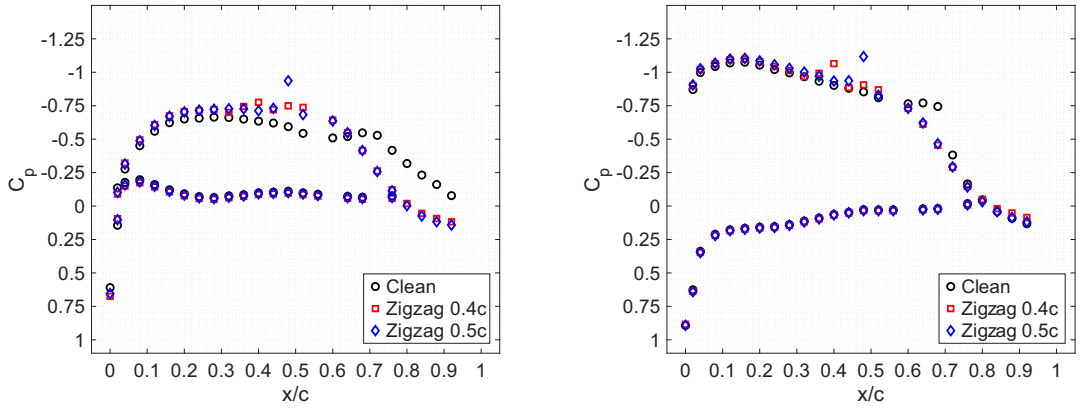
The differences in aerodynamic performance observed at the two Reynolds numbers can be further interpreted by examining the surface temperature distributions obtained from the InfraRed Thermography (IRT) measurements, together with the pressure coefficient distributions obtained from pressure tap measurements. Surface temperature distributions for $\mathrm{Re}_c = 2.5 \times 10^5$ at $\alpha = 1^\circ$ and 5° are shown in Fig. 7, while the corresponding pressure coefficient distributions are presented in Fig. 8.
At $\alpha = 1^\circ$ (Fig. 7a), the laminar boundary layer on the clean airfoil suction side separates at approximately $x/c = 0.54$. This is followed by a rapid increase in surface temperature, caused by the reduced convective heat transfer within the separated region. The further development of the separated shear layer is characterized by disturbance amplification and transition to turbulence, enhancing mixing and convective heat transfer downstream. This leads to a reduction in surface temperature and, in cases where reattachment occurs, results in a distinct local temperature minimum [3]. However, for the clean configuration at this angle of attack no such temperature minimum is observed, indicating that the flow does not reattach. Furthermore, the corresponding pressure coefficient distribution (Fig. 8a) shows a pronounced pressure plateau characteristic of separation, followed by an approximately linear pressure recovery, further confirming the absence of reattachment.



(a) $\alpha = 1^\circ$ (b) $\alpha = 5^\circ$

Figure 7 – Top: Surface temperature distributions for the clean airfoil and airfoil with zigzag tape for $\mathrm{Re}_c = 2,5 \times 10^5$. The symbols S, T, and R represent the locations of laminar separation, mean transition, and turbulent reattachment, respectively. Bottom: Corresponding spanwise-averaged surface temperature profiles. The shaded region denotes the unheated portion of the airfoil surface.

In the same figures, the effect of the zigzag tape is evident. The application of the trip significantly modifies the surface temperature distribution, eliminating the temperature rise associated with flow separation. Similar behaviour is observed in the pressure coefficient distribution. The tripped configuration exhibits increased suction levels over the range $x/c = 0.40$–0.60 and a more pronounced non-linear pressure recovery. These differences indicate a change in the flow topology, with separation occurring immediately downstream of the tape, followed by rapid transition to turbulence and early flow reattachment. As a result, the large separated region observed in the clean configuration is substantially reduced.

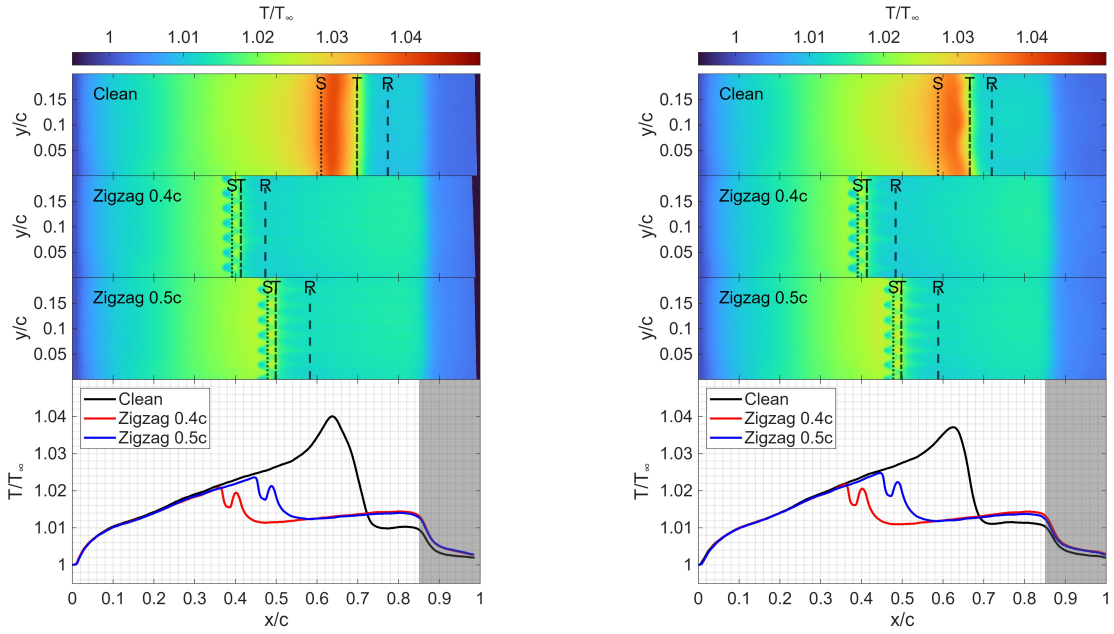


(a) $\alpha = 1^\circ$ (b) $\alpha = 5^\circ$

Figure 8 – Pressure coefficient distribution for $\mathrm{Re}_c = 2.5 \times 10^5$.

At $\alpha = 5^\circ$ (Figs. 7b and 8b), the flow over clean airfoil again separates at approximately $x/c = 0.54$, but in this case reattachment occurs at $x/c = 0.74$, resulting in the formation of an LSB. Flow reattachment is indicated by a nearly flat region in the surface temperature distribution and a non-linear pressure recovery in the C_p distribution. The resulting LSB extends over approximately 20% of the chord.
As in the previous case, the application of the zigzag tape significantly modifies this baseline be-

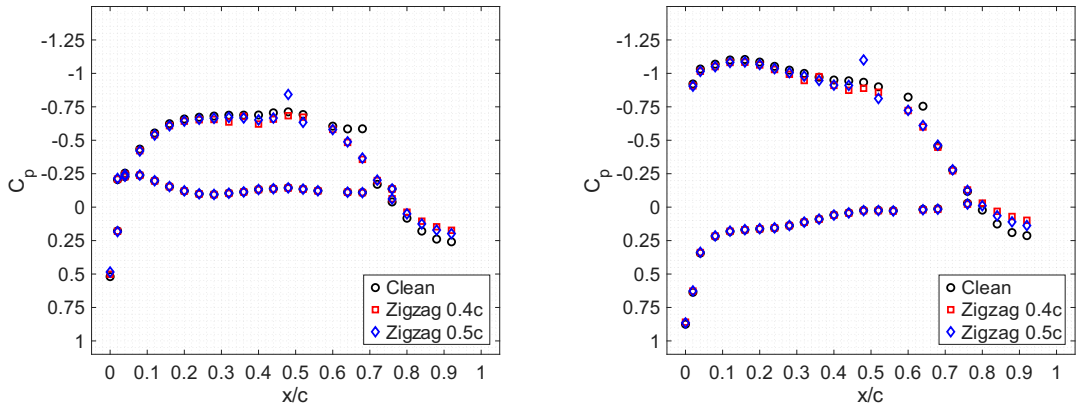
haviour by promoting earlier transition and reducing the extent of flow separation, as evidenced by both the surface temperature distributions and the pressure coefficient distribution. As a consequence the separated region is reduced from 20% of the chord to approximately 13% of the chord. Surface temperature and pressure coefficient distributions for $\mathrm{Re}_c = 5 \times 10^5$ at $\alpha = 1^\circ$ and 5° are presented in Figs. 9 and 10.



(a) $\alpha = 1^\circ$ (b) $\alpha = 5^\circ$

Figure 9 – Top: Surface temperature distributions for the clean airfoil and airfoil with zigzag tape for $\mathrm{Re}_c = 5 \times 10^5$. The symbols S, T, and R represent the locations of laminar separation, mean transition, and turbulent reattachment, respectively. Bottom: Corresponding spanwise-averaged surface temperature profiles. The shaded region denotes the unheated portion of the airfoil surface.

For both angles of attack, the flow over the suction side of the clean airfoil exhibits similar behaviour. From the surface temperature distributions in Fig. 9, it can be observed that the laminar boundary layer separates at approximately $x/c = 0.60$ and reattaches at approximately $x/c = 0.75$, forming an LSB that extends over approximately 13–14% of the chord. This interpretation is supported by the pressure coefficient distributions shown in Fig. 10, where separation is associated with a pressure plateau, while reattachment is indicated by a reduction in the pressure recovery rate.



(a) $\alpha = 1^\circ$ (b) $\alpha = 5^\circ$

Figure 10 – Pressure coefficient distribution for $\mathrm{Re}_c = 5 \times 10^5$.

In contrast to the $\mathrm{Re}_c = 2.5 \times 10^5$ case, the effects of the zigzag tape on the flow topology at $\mathrm{Re}_c = 5 \times 10^5$ are considerably less pronounced. From the surface temperature distributions, it can be

observed that the extent of the separated region is reduced only modestly, to approximately 10% of the chord. This limited influence is also evident in the pressure coefficient distributions, where the only notable difference between the clean and tripped configurations is a slight reduction in the extent of the pressure plateau associated with separation.
At this higher Reynolds number, the absence of a marked performance improvement can be attributed to the fact that the baseline flow is already only weakly affected by a laminar separation bubble. This is reflected in the surface temperature and pressure coefficient distributions, which show that the zigzag tape produces only a modest reduction in the extent of the separated region. Previous measurements on the same airfoil have further shown that increasing Reynolds number reduces both the length and thickness of the laminar separation bubble [19]. Consequently, the potential for drag reduction through forced transition is diminished, while the additional pressure and skin-friction drag introduced by the tripping device becomes relatively more significant. This interpretation is consistent with the aerodynamic performance results discussed in the previous section, where the benefits of tripping were found to diminish at $\mathrm{Re}_c = 5 \times 10^5$.

4. Conclusions

The influence of zigzag tape–induced transition on the aerodynamic performance and flow topology of the DU89-134 airfoil was investigated at $\mathrm{Re}_c = 2.5 \times 10^5$ and $\mathrm{Re}_c = 5 \times 10^5$ using force, pressure, and infrared thermography measurements.
The main findings are summarized as follows:

- At $\mathrm{Re}_c = 2.5 \times 10^5$, zigzag tape produced a substantial drag reduction while only marginally affecting lift, improving airfoil performance. This improvement was associated with a significant reduction in the extent of the suction-side separated region, attributed to effective tripping due to a near-optimal critical Reynolds number.
- At $\mathrm{Re}_c = 5 \times 10^5$, the influence of zigzag tape on aerodynamic performance was limited, with no measurable effect on the lift coefficient. The impact on drag was minimal, with differences in drag coefficient generally falling within the measurement uncertainty. A slight drag penalty was observed for the tripped configurations at higher angles of attack. This reduced effectiveness was attributed to the smaller extent of the laminar separation bubble in the baseline flow and the higher critical Reynolds number associated with the tripping device.
- No statistically significant differences were observed between the two investigated trip locations ($x/c = 0.4$ and $x/c = 0.5$) for both Reynolds numbers.

Overall, the results demonstrate that zigzag tape is an effective passive flow-control device. It was shown to effectively mitigate the adverse effects associated with low-Reynolds-number flow regime, leading to improved aerodynamic performance when the baseline flow is strongly affected by laminar separation.

5. Contact Author Email Address

Contact the corresponding author at: matija.avirovic@mil.be

6. Copyright Statement

The authors confirm that they, and/or their company or organization, hold copyright on all of the original material included in this paper. The authors also confirm that they have obtained permission, from the copyright holder of any third party material included in this paper, to publish it as part of their paper. The authors confirm that they give permission, or have obtained permission from the copyright holder of this paper, for the publication and distribution of this paper as part of the ICAS proceedings or as individual off-prints from the proceedings.

References

[1] H. Schlichting and K. Gersten. *Boundary-Layer Theory*. Springer, Berlin, Heidelberg, 9 edition, 2017.

[2] M. M. O'Meara and T. J. Mueller. Laminar separation bubble characteristics on an airfoil at low Reynolds numbers. *AIAA Journal*, 25(8):1033–1041, 1987.

[3] D. W. Wynnychuk and S. Yarusevych. Characterization of laminar separation bubbles using infrared thermography. *AIAA Journal*, 58(7):2831–2843, 2020.

[4] M. Miozzi, A. Capone, M. Costantini, L. Fratto, C. Klein, and F. Di Felice. Skin friction and coherent structures within a laminar separation bubble. *Experiments in Fluids*, 60(1):13, 2018.

[5] P. Lissaman. Low-Reynolds-number airfoils. *Annual Review of Fluid Mechanics*, 15:223–239, 1983.

[6] A. Mitra, P. Gokul, and O. N. Ramesh. The role of laminar separation bubble on low Reynolds number airfoils. In *51st AIAA Aerospace Sciences Meeting Including the New Horizons Forum and Aerospace Exposition*, 2013.

[7] A. Gopalarathnam, B. A. Broughton, B. D. McGranahan, and M. S. Selig. Design of low Reynolds number airfoils with trips. *Journal of Aircraft*, 40(4):768–775, 2003.

[8] Y. Patel and P. J. Ansell. Airfoil performance sensitivity to laminar separation bubble topology. *AIAA AVIATION 2023 Forum*, 2023.

[9] R. P. J. O. M. van Rooij and W. A. Timmer. Roughness sensitivity considerations for thick rotor blade airfoils. *Journal of Solar Energy Engineering*, 125(4):468–478, 2003.

[10] C. Brunelli, M. Avirovic, B. Janssens, B. G. Marinus, and M. Runacres. Numerical and experimental study of effects of triangular cross-section riblets on DU89-134 airfoil. *Aerotecnica Missili & Spazio*, 2025.

[11] C. Lyon, M. S. Selig, and A. Broeren. Boundary layer trips on airfoils at low Reynolds numbers. In *35th AIAA Aerospace Sciences Meeting and Exhibit*, 1997.

[12] Peter Scholz and Lajos Fohlmeister. Measurement of boundary layer properties downstream of a transition trip. In *19th International Symposium on the Application of Laser and Imaging Techniques to Fluid Mechanics*, 2018.

[13] F. L. dos Santos, M. P. Sanders, L. D. de Santana, and C. H. Venner. Influence of tripping devices in hastening transition in a flat plate submitted to zero and favorable pressure gradients. *AIAA Scitech 2020 Forum*, 2020.

[14] Jin Zhang, Jin Zhang, Lajos Fohlmeister, and Peter Scholz. Large-Eddy Simulation of Boundary-Layer Transition over a Zigzag Trip. *AIAA Journal*, 61(3):1032–1047, 2023.

[15] G. E. Elsinga and J. Westerweel. Tomographic-PIV measurement of the flow around a zigzag boundary layer trip. *Experiments in Fluids*, 52(4):865–876, 2012.

[16] Q. Ye, F. Avallone, D. Ragni, M. Choudhari, and D. Casalino. Effect of surface roughness geometry on boundary-layer transition and far-field noise. *AIAA Journal*, 59(7):2396–2408, 2021.

[17] F. L. dos Santos, C. H. Venner, and L. D. de Santana. Tripping device effects on the turbulent boundary layer development. In *AIAA AVIATION 2022 Forum*. AIAA, 2022.

[18] L. M. M. Boermans and A. van Garrel. Design and windtunnel test results of a flapped laminar flow airfoil for high-performance sailplane applications. In *The International Council of the Aeronautical Sciences Congress*, Anaheim, 1994.

[19] M. Avirovic, C. Brunelli, B. G. Marinus, J. Degroote, and J. van Beeck. Laminar–Turbulent Transition on a DU89-134/14 Airfoil at Low Reynolds Number. *AIAA Journal*, 2026.

[20] Carlo Brunelli, Matija Avirovic, Bart Janssens, Benoît G. Marinus, Koen Hillewaert, and Mark Runacres. Prediction of laminar separation bubble on airfoils at low reynolds number. *Flow, Turbulence and Combustion*, 116(2):27, 2026.

[21] M. Avirovic, C. Brunelli, B. Marinus, J. Degroote, and J. Van Beeck. Laminar-turbulent transition on a DU89-134 airfoil at low reynolds number for use at high altitude. In *AIAA Aviation Forum and Ascend 2024*, 2024.

[22] A. L. Braslow and E. C. Knox. Simplified method for determination of critical height of distributed roughness particles for boundary-layer transition at mach numbers from 0 to 5. Technical report, National Advisory Committee for Aeronautics, 1958.

[23] J.B. Barlow, W.H. Rae, and A. Pope. *Low-Speed Wind Tunnel Testing*. John Wiley and Sons, 3rd edition edition, 1999.

[24] H.K. Yuen, J Princen, J Illingworth, and J Kittler. Comparative study of Hough transform methods for circle finding. *Image and Vision Computing*, 8(1):71–77, 1990.